Electronic Supplementary Material (ESI) for Nanoscale

Mechanics and Molecular Filtration Performance of Graphyne Nanoweb Membranes for Selective Water Purification

Shangchao Lin and Markus J. Buehler*

Laboratory for Atomistic and Molecular Mechanics (LAMM), Department of Civil and Environmental Engineering, Massachusetts Institute of Technology, Cambridge, Massachusetts 02139, United States

**Corresponding Author: E-mail: mbuehler@MIT.EDU*

Electronic Supplementary Information (ESI)

Table S1. Non-bonded (LJ and Coulombic) force field parameters employed in this work.

Element	σ (Å)	ε (kJ/mol)	q (e)
C (Graphyne and Graphene)	3.40000	0.223049	0
H (Water)	0	0	0.4238
O (Water)	3.16557	0.650194	−0.8476
Cu^{2+}	2.08470	4.76976	2
S (SO_4^{2-})	3.56000	1.65268	1.52
O (SO_4^{2-})	2.96000	0.711280	−0.88
C (C_6H_6)	3.55000	0.292880	−0.115
H (C_6H_6)	2.42000	0.125520	0.115
C (CCl_4)	3.80000	0.209200	0.248
Cl (CCl_4)	3.47000	1.11295	−0.062
Na^+	3.33045	0.011598	1
Cl^-	4.41724	0.492833	−1

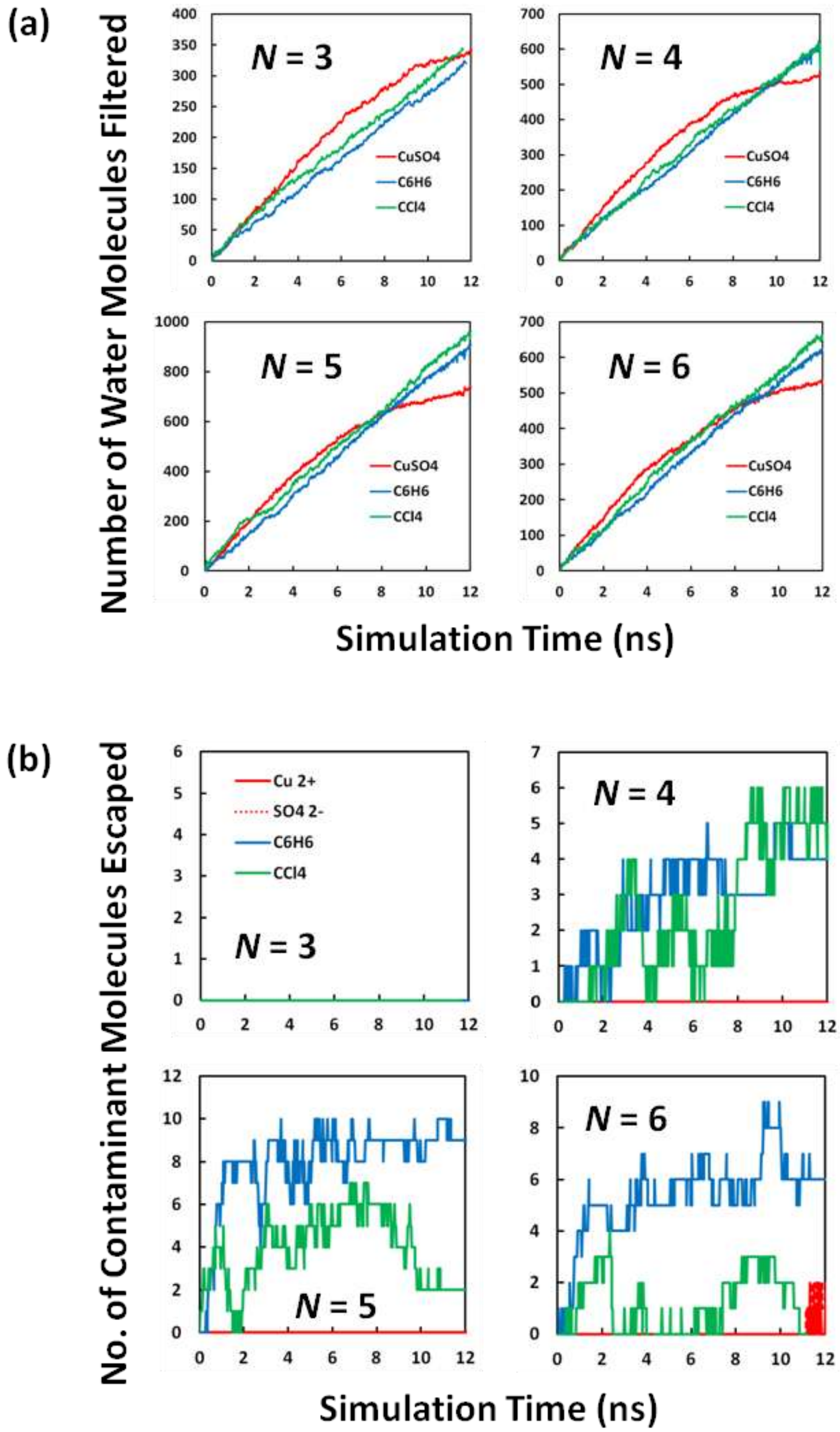

Figure S1. (a) Water transport dynamics through various graphyne membranes ($N = 3 \sim 6$) when filtering contaminants ($CuSO_4$, C_6H_6, and CCl_4) under a fixed hydrostatic pressure $\Delta P = 50$ MPa. **(b)** Transport dynamics of the contaminants during the filtration simulation, corresponding to **(a)**.

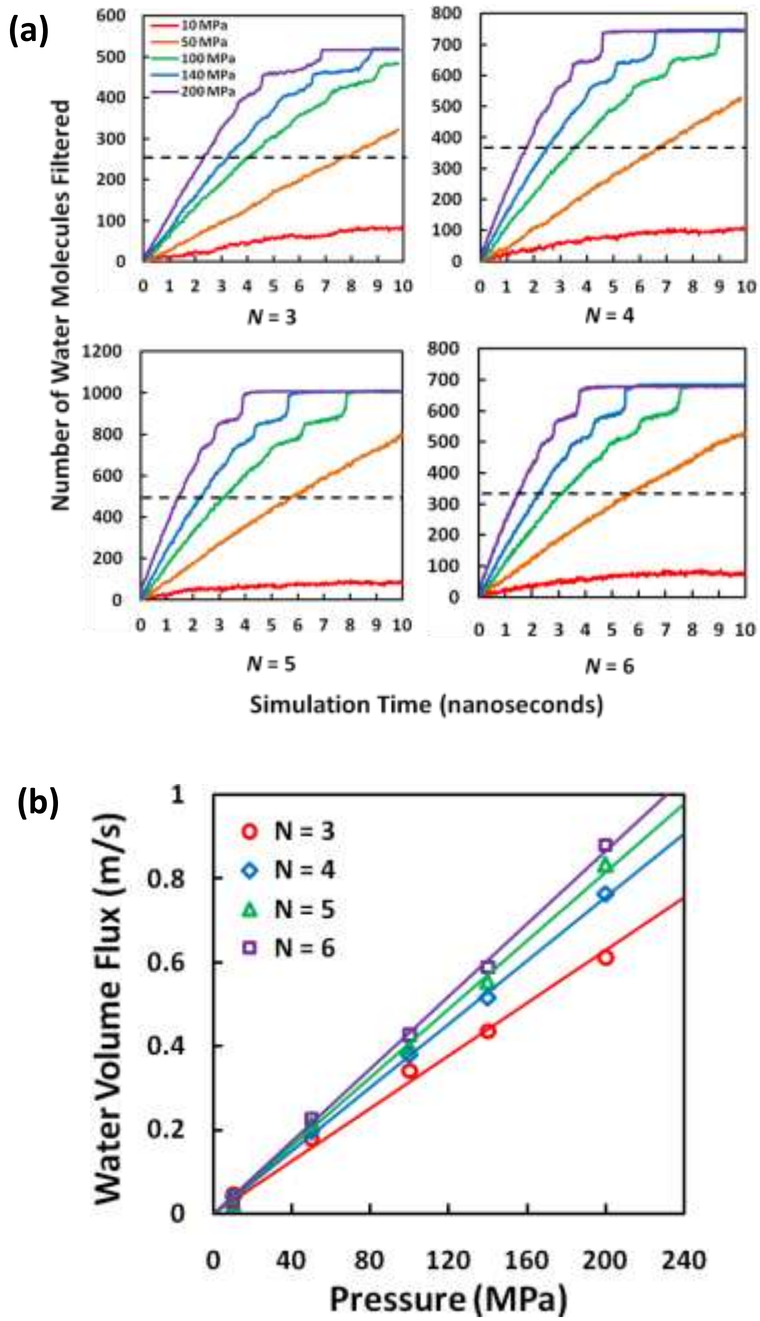

Figure S2. (a) Salt water transport dynamics through various graphyne membranes (N = 3 ~ 6) under different hydrostatic pressures. The profiles show that the water flux is constant in time when less than half of the saline water has been filtered (region below the black dashed line in each subplot). In addition, the water flux also increases with N (or effective pore diameter, D) and the applied pressure ΔP. The legend on top left applies to all four subplots. **(b)** Linear behavior of the water volume fluxes J_{water}, through various graphyne membranes (N = 3 ~ 6) with respect to the hydrostatic pressure. The water flux is extrapolated from the linear region of the curves in **(a)** (below the black dashed lines) and normalized by the cross-sectional area of the corresponding simulation unit cell. The solid lines are linear fittings.

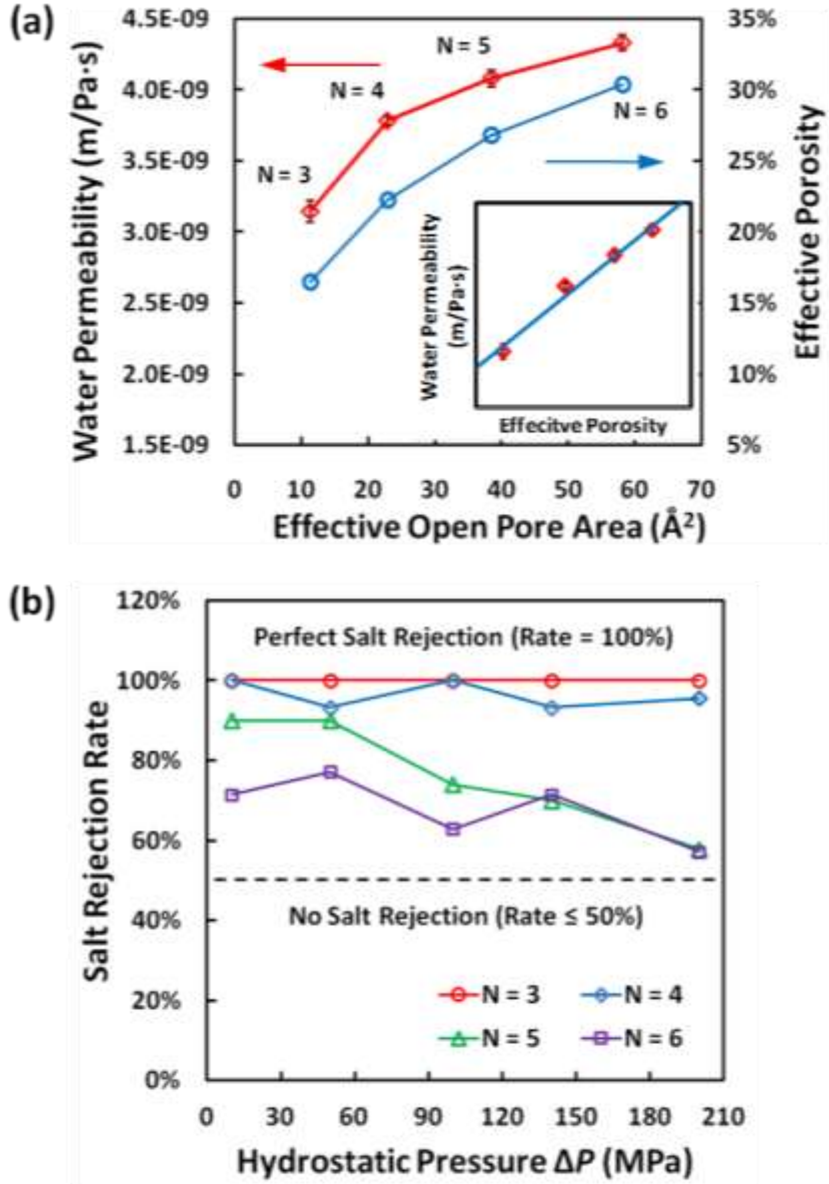

Figure S3. (a) Salt water permeabilities and effective membrane surface porosities, φ, for the various graphyne membranes as a function of the effective open pore areas, a. The error bars are from the standard deviations of the linear fitting process in **Fig. S2(b)**. The inset shows the linear behavior of water permeabilities with respect to φ. The solid blue line is the linear fitting. **(b)** Salt rejection rates (based on total salt masses), η, through graphyne membranes under different hydrostatic pressures ΔP.

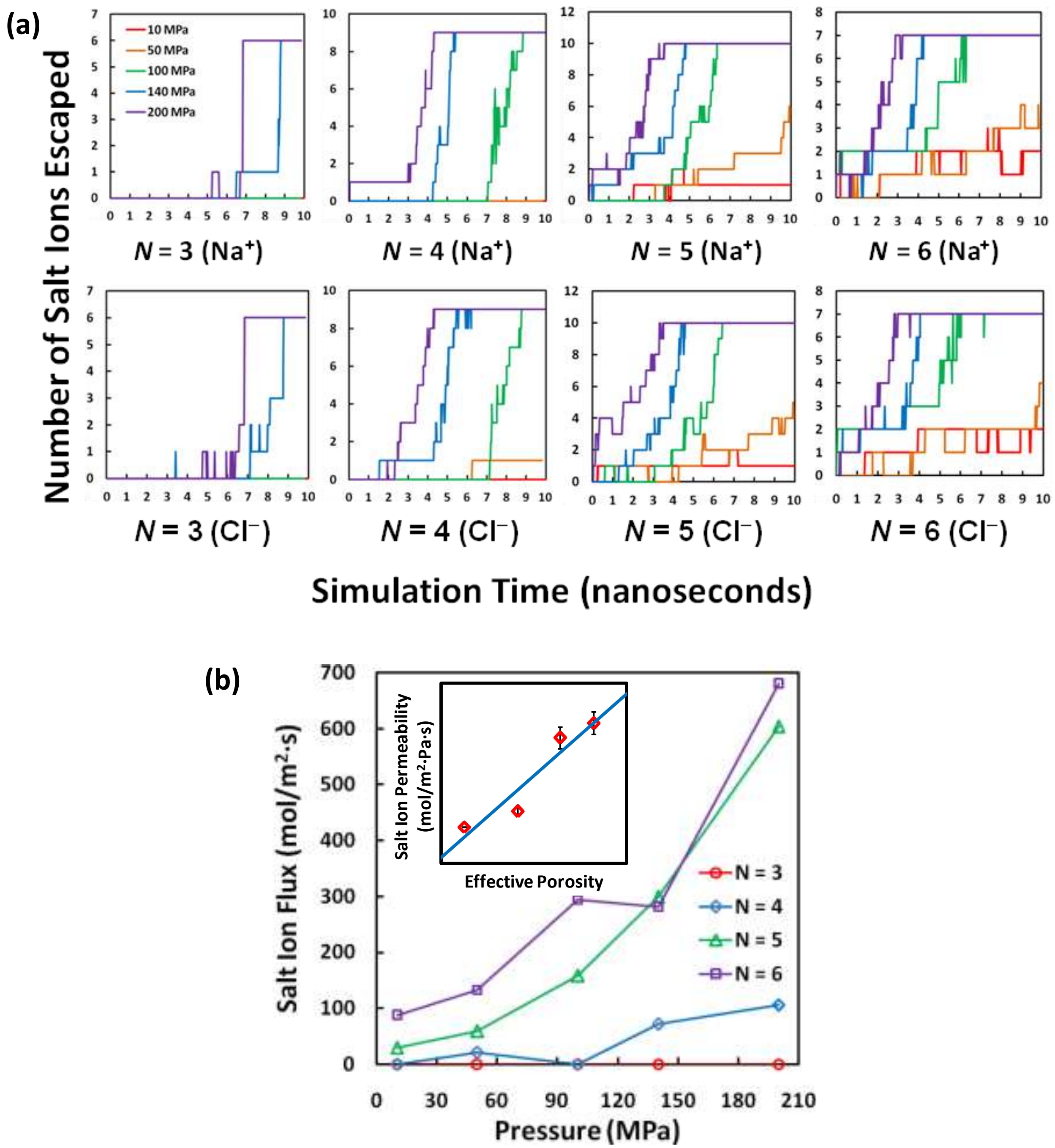

Figure S4. (a) Salt ion transport dynamics through graphyne membranes under different hydrostatic pressures. Similar to the water flux in **Fig. S2(b)**, salt ion flux also increases with N and the applied pressure ΔP. The legend on top left applies to all eight subplots. **(b)** Salt ion flux (Na^+ plus Cl^-), J_{salt}, through graphyne membranes under different hydrostatic pressures. The inset shows the close-to-linear behavior of the salt ion permeability, M_{salt}, with respect to the effective membrane surface porosity, φ. The values of M_{salt} and the associated errors are computed using the same method for determining water permeabilities in **Fig. S3(a)**.

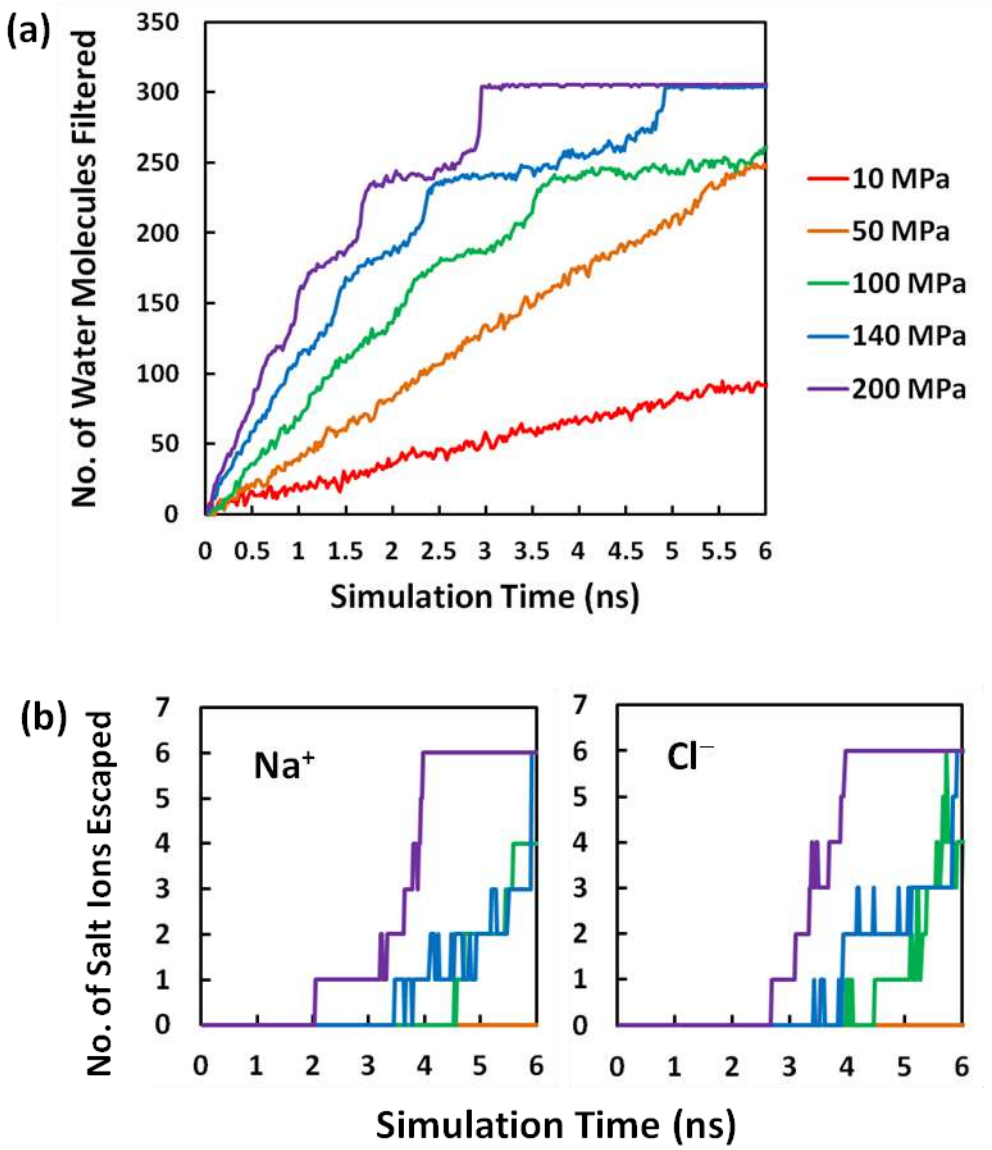

Figure S5. Impact from mechanical deformations to the desalination performance of the graphtriyne membrane under the ultimate strain of 1.6%. **(a)** Water transport dynamics through the deformed graphtriyne membranes under different hydrostatic pressures. **(b)** Salt ion transport dynamics through the deformed graphtriyne membranes under different hydrostatic pressures. The legend in **(a)** applies to **(b)** as well.